A compressive-sensing Fourier-transform spectrometer chip using subwavelength grating waveguides

HUGH PODMORE[1,*], ALAN SCOTT[2], PAVEL CHEBEN[3], AITOR V. VELASCO[4], JENS H. SCHMID[3], MARTIN VACHON[3], AND REGINA LEE[1]

[1] Department of Physics and Astronomy, York University, 4700 Keele St, Toronto, ON, M1J 1P3
[2] Honeywell Aerospace, 303 Terry Fox Dr, Kanata, ON
[3] National Research Council of Canada, 1200 Montreal Rd, Ottawa, ON
[4] 4Spanish National Research Council (CSIC), Madrid, Spain
[*] Corresponding author: podmore@yorku.ca

Compiled January 18, 2017

We propose a novel formulation of planar-waveguide Fourier-transform spectrometers (FTS) as a vehicle for compressive-sensing (CS) spectroscopy. These spectrometers consist of a set of independent Mach Zehnder interferometers (MZIs) formed from optical waveguides printed on a photonic chip. The signal from a set of MZIs comprises an undersampled discrete Fourier interferogram, which may be inverted using l1-norm minimization to retrieve an input spectrum that is assumed to be sparse. We use a subwavelength-engineered spatially-heterodyned Fourier-transform spectrometer (SHFTS) on a chip consisting of 32 independent MZIs to demonstrate this principle. We successfully demonstrate the retrieval of three sparse input signals by collecting data from 14 or fewer MZIs and applying common CS reconstruction techniques to this data. We demonstrate that this retrieval maintains the full resolution and bandwidth of the original device despite a sampling factor as low as 1/4th that of non-compressive designs.

OCIS codes: *(130.0130) Integrated optics; (070.2025) Discrete optical signal processing; (120.6200) Spectrometers and spectroscopic instrumentation; (300.6310) Spectroscopy, heterodyne; (300.6300) Spectroscopy, Fourier transforms; (350.4238) Nanophotonics and photonic crystals*

http://dx.doi.org/10.1364/ao.XX.XXXXXX

1. INTRODUCTION

Miniature spectrometers are an invaluable tool in many applications including environmental sensing, biology, medical diagnostics, geology, security, and planetary science [1, 2]. They are particularly sought after in space instrumentation and planetary exploration where it is desirable to minimize the mass and volume of all instruments—without compromising performance. In particular, miniature spectrometers are often deployed for the purposes of Raman spectroscopy, a fundamental technique for exominerology and exobiology [3]. One promising platform for the design of miniature spectrometers is planar waveguide photonic chips [4]. In such a system, light is collected and routed through either a dispersive element (DE) [5] or a set of interferometers as in Fourier-transform spectroscopy (FTS) [6].

Of these two architectures, FTS devices are preferred for their higher optical throughput and resolving power when compared with DE-type spectrometers [4, 7]. FTS devices may be realized in planar-waveguides using a set of Mach Zehnder interferometers (MZIs) with linearly increasing path delays [7, 8]. Such a system constitutes a spatially heterodyning Fourier-transform spectrometer (SHFTS). In an SHFTS each point in the interferogram—corresponding to the output of a particular MZI—is captured independently by a linear detector array, allowing for interferogram acquisition in a single shot. Limits on detector size and fabrication capabilities place constraints on the number of MZIs that may be placed on a single photonic chip, ultimately limiting the bandwidth and/or the resolution of an SHFTS chip. An SHFTS is unlike a scanning FTS [9], where the interferogram is heterodyned in the temporal domain and captured by a single detector running at a high readout rate.

Compressive-sensing (CS) techniques are highly applicable to FTS devices [10]; providing a compelling path towards reducing the number of MZIs on a planar-waveguide chip. In a CS scheme, the input signal is assumed to be sparse, and this assumption is used to leverage a reduction in the number of sampling points—or MZIs—required to correctly retrieve the input signal. CS schemes translate well to Fourier-transform devices as the sensing basis (frequency) and the measurement basis (temporal) are maximally incoherent, meaning that a sparse signal in the frequency domain will produce a non-zero signal level at all points in the time-domain [11]. Furthermore, CS schemes are particularly well suited to SHFTS devices as the sampling points in the interferogram are collected independently. Therefore, re-

ducing the number of samples in an SHFTS can have a significant impact on the footprint of the chip. For instance, a discretely sampled interferogram consisting of M data points—corresponding to M MZIs—may be reduced to a subset of $K < M$ sampling points with no loss in information. This advantage cannot be realized in a scanning FTS, which necessarily collects the full set of sampling points in the time-domain.

In this paper we combine CS reconstruction techniques with a FTS realized using planar-waveguide technology in order to demonstrate enhanced bandwidth with a reduced number of MZIs. CS FTS devices of this type present an enabling technology for miniaturized Raman spectrometers, as Raman spectra exhibit a high degree of sparsity [12].

2. SUBWAVELENGTH GRATING PLANAR WAVEGUIDE FTS

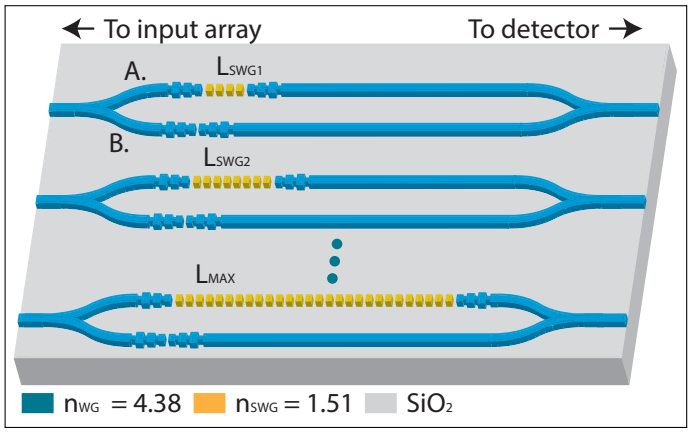

Fig. 1. (Colour online) Light from the spectrometer aperture is directed to an array of interferometers each consisting of a 50:50 splitter a delay arm (A) and reference arm (B). The delay arm in the $i-$th interferometer consists of a pair of subwavelength mode-converters and a SWG region characterized by length L_{SWGi}. The reference arm consists of an identical set of mode-converters, and has a fixed length of 1.5 cm.

The planar-waveguide spectrometer used in this work consists of 32 unbalanced MZIs with linearly increasing optical path delays (OPDs), as illustrated in figure 1. The OPDs are produced via engineering a change in the optical propagation constant β between the two arms of the MZI, rather than by introducing a geometrical path difference. One arm of each MZI consists of standard Si-wire waveguides, while the other arm is formed from a subwavelength grating (SWG), that is, a periodic array of Si slabs with spacing less than the optical wavelengths of interest. SWG may be considered as an optical metamaterial with a propagation constant that is controlled by the periodicity and the duty-cycle of the grating [13].

The MZIs are fabricated on a wafer consisting of a Si substrate, buried oxide layer, a 260 nm thick Si layer from which waveguides are formed, and an SU-8 upper cladding. The Si-wire waveguide width is 450 nm, while the SWG grating has width 300 nm, grating periodicity 400 nm, and a 50% grating fill-factor. This results in a group index of the subwavelength region of $n_{SWG} = 1.51$, and a group index for the waveguide region of $n_{WG} = 4.38$. The mismatch in group index between the two MZI arms generates the desired phase imbalance, controlled along the array by increasing or decreasing the length of the subwavelength region in the delay arm.

The first OPD in the set of MZIs is $L_{SWG1} = 470^{-}$m, the second OPD is $2L_{SWG1} = 940^{-}$m, the third $3L_{SWG1}$, and so on, up to a maximum OPD of $L_{max} = 1.5$ cm. The wavenumber-dependent output of each MZI is a cosine transform of the input spectra; the full complement of these MZIs thus constituting a discretely-sampled inverse Fourier-transform of the input spectra. The theoretical resolution, $\delta\lambda$, and bandwidth, $\Delta\lambda$, of the device are given by

$$\delta\lambda = \frac{\lambda_0^2}{L_{max}}(n_{WG} - n_{SWG}) \quad (1)$$

$$\Delta\lambda = \delta\lambda\frac{M}{2}. \quad (2)$$

Where λ_0 is the central wavelength of the device (1550.5 nm), and M is the total number of MZIs in the device [8]. Experimentally, the resolution and bandwidth of the device are found to be $\delta\lambda = 48$ pm, and $\Delta\lambda = 0.78$ nm [13], in good agreement with the theoretical values.

A key advantage of defining the OPD of each MZI through a change in index rather than a change in the physical path length is that the fringe visibility of the MZIs, and hence overall device sensitivity, is greatly enhanced. Fringe visibility is a product of the overall optical efficiency of the device, as well as the imbalance in optical efficiency between MZI arms. The fringe visibility ν is defined by the contrast in modulation between the maximum and minimum output signals of each MZI I_{max}, and I_{min}:

$$\nu = \frac{I_{max} - I_{min}}{I_{max} + I_{min}}. \quad (3)$$

The observed fringe maxima and minima in a particular MZI will be defined by the propagation losses α, as well as the physical path lengths of the two arms, z. In the subwavelength device, there is no physical path difference between the arms, therefore the fringe visibility is controlled entirely by the difference in propagation loss between the SWG and wire waveguides. In this device the losses are well balanced: loss in the SWG region is $\alpha_{SWG} = -3.0$ dB/cm, while the loss in the waveguide region is given by $\alpha_{WG} = -3.1$ dB/cm. Experimentally, we find a mean visibility factor $\bar{\nu} = 0.96$.

3. EXPERIMENTAL SPECTRAL RETRIEVAL

A high-resolution tuneable laser source was used to characterize the response of the subwavelength waveguide spectrometer. The excitation wavelength was steadily incremented in 5 pm steps over the FSR of the device, while the input power was held constant at 1mW. The input light was restricted to the transverse magnetic polarization state (TM), and coupled to the spectrometer via a lensed fiber. The input power was split equally and routed to the individual MZIs using cascaded Y-splitters. The output signal from each output was collimated using a high numerical aperture (NA) microscope objective, and captured using a calibrated InGaAs camera. Throughout this procedure, the chip temperature was stabilized through the use of a Peltier stage. The product of this characterization procedure is an $M \times N$ transformation matrix, $\mathbf{\Phi}$, in which M is the number of waveguide outputs, and N is the number of measured discrete wavelength points. The matrix obtained from the particular SWG instrument under analysis is displayed in figure 2. Each row in this matrix, also called a spectral or calibration map, contains the phase and frequency modulation information for a

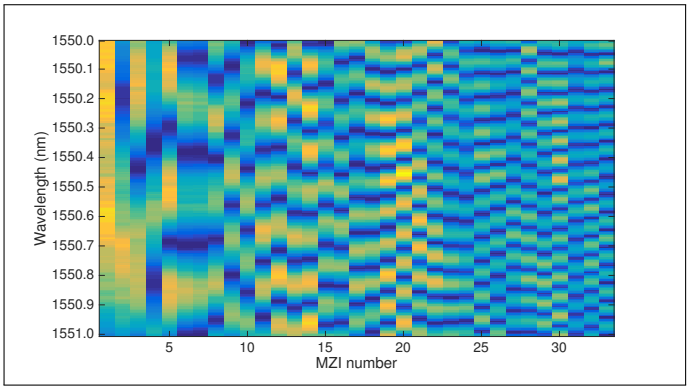

Fig. 2. (Colour online) Transpose of experimentally-obtained characterization matrix of SWG FTS displaying the wavelength-dependent output power of each of the 32 MZIs as obtained in a high-resolution wavelength scan across 1 nm centered at 1550.5 nm.

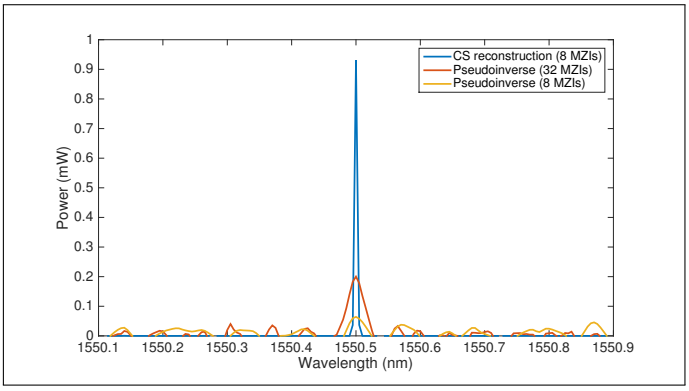

Fig. 3. (Colour online) Spectra from narrow-band laser source with 1 mW input power retrieved using un-apodized interferometric measurements obtained from the MZIs. A subset of 8 MZIs is randomly selected and their output intensities are used to retrieve the laser spectrum via l1-norm minimization (blue). The spectrum is also reconstructed via pseudoinverse methods using the full complement of 32 MZIs (orange), as well as the same subset of 8 MZIs as in the CS retrieval (yellow).

single MZI in the spectrometer. The matrix in its entirety can be used to retrieve an input spectrum via its pseudoinverse [8].

This calibration matrix may also be used to define a CS scheme, wherein an unknown, sparse input spectrum, x, produces an output signal, y, via the sensing scheme

$$y = \mathbf{A}x. \tag{4}$$

In this formulation, $\mathbf{A}$ is a $K \times N$ matrix with $K < M$ that satisfies the restricted isometry property (RIP); i.e. the columns in A must be approximately orthogonal. Randomly selected rows of a Fourier-transform matrix are known to satisfy the RIP, hence a set of K randomly selected MZIs will suffice to define $\mathbf{A}$ while satisfying the RIP [14]. Selecting a subset of K rows from the calibration matrix is equivalent to measuring the outputs of only those same MZIs, while ignoring the remaining MZIs. Once the output signals of the K-selected MZIs have been collected, equation 4 may be solved via l1-norm minimization, basis-pursuit, or any other CS reconstruction technique to return the original input spectrum x. In this work the full set of M MZIs is present on the chip for the purposes of establishing a baseline comparison. However, an actual CS spectrometer consisting of only the K-selected subset of MZIs could also be fabricated.

First we consider the case of a monochromatic input spectrum defined by a narrow-band laser source centered at $\lambda_0 = 1550.5$ nm with 1 mW input power. 8 MZIs are selected randomly from the instrument set, their output values are recorded, and the input spectrum is retrieved through l1-norm minimization via basis-pursuit denoising [10]. This spectrum is shown in figure 3 alongside a retrieval obtained using the pseudoinverse of the calibration map, $\mathbf{\Phi}$, as well as the pseudoinverse of $\mathbf{A}$. The retrieval obtained via l1-norm minimization lacks the hyperbolic sinusoid associated with the instrumental lineshape of a FTS device, but is otherwise in agreement with the result obtained via the pseudoinverse of the full-complement of MZIs. The lack of an instrument lineshape in a CS FTS is to be expected, as CS schemes assume a-priori that the input spectra is sparse. We find that the spectra retrieved via l1-norm minimization of A successfully reconstructs the laser line despite undersampling the interferogram by an undersampling factor $c = 0.25$. By contrast, it is not possible to retrieve a meaningful spectra from the same 8 MZIs using the pseudoinverse of $\mathbf{A}$ since the interferogram is too heavily undersampled for non-CS methods. We note that the total power retrieved in all three methods is consistent with 1 mW when integrated across wavelength, i.e. the optical power is not lost in the pseudoinverse retrieval, it is merely redistributed to the line widening and sidelobes.

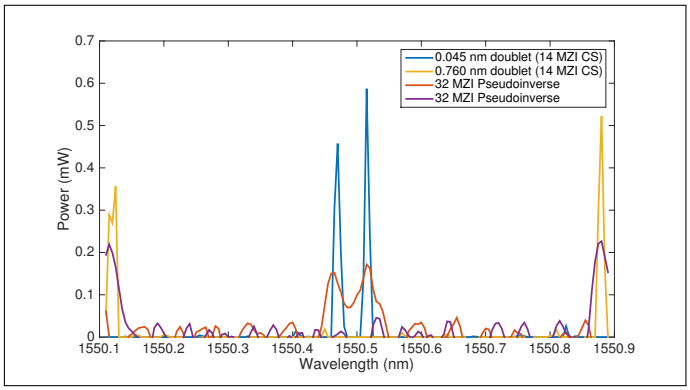

Fig. 4. (Colour online) Spectra from two doublets, with peak-to-peak separation of 0.045 nm and 0.76 nm, retrieved using un-apodized interferometric measurements obtained from the MZIs. A subset of 14 MZIs is randomly selected and their output intensities are used to retrieve the spectra via l1-norm minimization (blue, yellow). The spectra are also reconstructed via pseudoinverse methods using the full complement of 32 MZIs (orange, purple).

We also consider retrieval of two polychromatic spectra each consisting of two 1 mW monochromatic sources, one separated by 0.045 nm, and the other by 0.76 nm. The narrow appearances of the spectral features retrieved in figure 3 do not imply that the CS FTS retrieval produces higher spectral resolution than the pseudoinverse retrieval. On the contrary, narrow spectral features are a straightforward consequence of the initial sparsity assumption of the CS methods. The resolution limit, defined by the minimum peak-to-peak separation of a doublet that can be resolved by the device is still well described by the

Shannon-Nyquist theorem [15]. Retrieval of a polychromatic doublet is shown in figure 4. The first doublet separation is 0.045 nm, which is consistent with the expected Nyquist resolution of the device, 0.048 nm. A second doublet retrieval with separation equal to the bandwidth of the device, 0.76 nm, is also shown in order to demonstrate preservation of bandwidth. As in the case of the monochromatic case, it was not possible to retrieve the spectra of either doublet using the pseudoinverse of **A**, as the interferogram produced by the 14 MZIs is too heavily undersampled for non-CS methods.

The results presented in figure 3 and figure 4 demonstrate that the bandwidth and resolution of the compressive sensing spectrometer are identical to the original spectrometer. The CS FTS, however, requires only 14 MZIs to the original 32 in the case of a doublet (undersampling factor $c = 0.44$), and only 8 MZIs to retrieve a monochromatic source (undersampling factor $c = 0.25$). The reduction in the number of sampling points comes at a cost: the CS spectrometer cannot retrieve a white-light or broadband spectrum as the signal is no longer sparse. There are, however, a large number of naturally occurring sparse spectra of interest to scientists. Both Raman and laser-induced breakdown spectroscopy (LIBS) are techniques that produce sparse input signals. Strong spectral emission or absorption lines of interest to atmospheric scientists and astronomers may also be considered sparse if a suitable background removal scheme is applied. Optical characterization devices used in high-precision metrology, such as wavemeters, may analyze only one or two laser lines at a time—a very high degree of sparsity.

The results presented in figure 3 and figure 4 demonstrate that the bandwidth and resolution of the compressive sensing spectrometer are identical to the original spectrometer. The CS FTS, however, requires only 14 MZIs to the original 32 in the case of a doublet (undersampling factor $c = 0.44$), and only 8 MZIs to retrieve a monochromatic source (undersampling factor $c = 0.25$). The reduction in the number of sampling points comes at a cost: the CS spectrometer cannot retrieve a white-light or broadband spectrum as the signal is no longer sparse. There are, however, a large number of naturally occurring sparse spectra of interest to scientists. Both Raman and laser-induced breakdown spectroscopy (LIBS) are techniques that produce sparse input signals. Strong spectral emission or absorption lines of interest to atmospheric scientists and astronomers may also be considered sparse if a suitable background removal scheme is applied. Optical characterization devices used in high-precision metrology, such as wavemeters, may analyze only one or two laser lines at a time—a very high degree of sparsity.

4. CONCLUSIONS

In this paper we propose a novel formulation of on-chip FTS devices as a vehicle for CS spectroscopy. We contend that the spatial heterodyne configuration of on-chip FTS devices, consisting of a set of independent interferometers, is uniquely well-suited to CS spectroscopy. We use a subwavelength-engineered SHFTS on a photonic chip consisting of 32 independent MZIs to demonstrate this principle experimentally. We use subwavelength-engineering in the interferometer arms to balance the propagation losses and enhance the fringe visibility of the device. We take advantage of the spatial-heterodyne configuration to independently sample the MZIs, and selectively downsample the interferogram. Using 8 out of the original 32 MZIs, we successfully demonstrate the retrieval of a singlet; using 14 MZIs we successfully retrieve two doublets, maintaining the full resolution and bandwidth of the original device.

These results validate our underlying thesis: that CS schemes may be deployed on SHFTS chips in order to enable a substantial reduction in the number of MZIs required to produce a functional spectrometer. This result may have future application in the pursuit of smaller and more capable chip spectrometers. For instance, a CS spectrometer of this type may be designed to achieve the same bandwidth and resolution as a fully-sampled device with a much smaller footprint on-chip. Miniaturized CS FTS devices, such as the devices described herein, would be suitable for characterization of optical equipment and for measuring naturally occurring sparse signals, such as Raman and LIBS emission spectra, and atmospheric absorption and emission spectra.

5. FUNDING INFORMATION

This work was supported by Honeywell Aerospace, as well as funding by the Canadian Space Agency (CSA), and the Natural Sciences and Engineering Research Council of Canada (NSERC). The authors acknowledge Przemek Bock for simulation and mask preparation, and Jean Lapointe for e-beam patterning. Aitor V. Velasco acknowledges support from Spanish Ministry of Economy through project TEC2015-71127-C2 and FJCI-2014-22836, Community of Madrid through project S2013/MIT-2790, and EURAMET through project JRP-i22 14IND13-PhotInd and H2020-MSCA-RISE-2016: SENSIBLE. EMPIR initiative is co-funded by the European Union's Horizon 2020 research and innovation programme and the EMPIR participating states.

REFERENCES

1. C. P. Bacon, Y. Mattley, and R. DeFrece, Review of Scientific instruments **75**, 1 (2004).
2. A. D. Scott, N. Rowlands, and A. Bell, Proceedings of SPIE **5660**, 78 (2004).
3. J. Blacksberg, E. Alerstam, Y. Maruyama, C. J. Cochrane, and G. R. Rossman, Applied Optics **55**, 739 (2016).
4. M. Florjańczyk, P. Cheben, S. Janz, B. Lamontagne, J. Lapointe, A. Scott, B. Solheim, and D.-X. Xu, Proceedings of SPIE **7594**, 75940R (2010).
5. X. Ma, M. Li, and J. J. He, IEEE Photonics Journal **5**, 6600807 (2013).
6. K. Okamoto, H. Aoyagi, and K. Takada, Optics Letters **35**, 2103 (2010).
7. M. Florjańczyk, P. Cheben, S. Janz, A. Scott, B. Solheim, and D.-X. Xu, Optics Express **15**, 18176 (2007).
8. A. V. Velasco, P. Cheben, P. J. Bock, A. Delâge, J. H. Schmid, J. Lapointe, S. Janz, M. L. Calvo, D.-X. Xu, M. Florjańczyk, and M. Vachon, Optics Letters **38**, 706 (2013).
9. M. Erfan, Y. M. Sabry, M. Sakr, B. Mortada, M. Medhat, and D. Khalil, Applied Spectroscopy **70**, 897 (2016).
10. E. van den Berg and M. P. Friedlander, SIAM Journal on Scientific Computing **31**, 890 (2008).
11. E. J. Candes and M. B. Wakin, IEEE Signal Processing Magazine **25**, 21 (2008).
12. O. Katz, J. M. Levitt, and Y. Silberberg, Frontiers in Optics 2010/Laser Science XXVI p. FTuE3 (2010).
13. P. J. Bock, P. Cheben, A. V. Velasco, J. H. Schmid, A. Delâge, M. Florjańczyk, J. Lapointe, D.-X. Xu, M. Vachon, S. Janz, and M. L. Calvo, Laser & Photonics Reviews **7**, L67 (2013).
14. M. Fornasier, *Theoretical foundations and numerical methods for sparse recovery*, vol. 9 (Walter de Gruyter, 2010).
15. H. Nyquist, Transactions of the American Institute of Electrical Engineers **47**, 617 (1928).